Electronic Supplementary Information

Supramolecular organization of melem for the synthesis of photoactive porous carbon nitride rods

Jiawei Xia,[a,b] Gabriel Mark,[b] Michael Volokh,[b] Yuanxing Fang,[c] Haiqun Chen,[a] Xinchen Wang[c] and Menny Shalom[b]*

[a]Key Laboratory of Advanced Catalytic Materials and Technology, Advanced Catalysis and Green Manufacturing Collaborative Innovation Center, Changzhou University, Changzhou, Jiangsu Province 213164, China.

[b]Department of Chemistry and Ilse Katz Institute for Nanoscale Science and Technology, Ben-Gurion University of the Negev, Beer-Sheva 8410501, Israel.
E-mail: mennysh@bgu.ac.il

[c]State Key Laboratory of Photocatalysis on Energy and Environment College of Chemistry, Fuzhou University, Fuzhou 350116, China

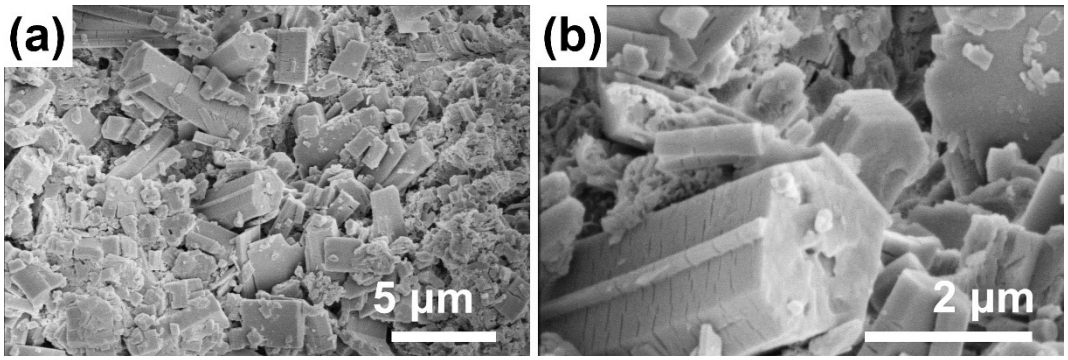

Fig. S1 SEM images of Me at different magnifications.

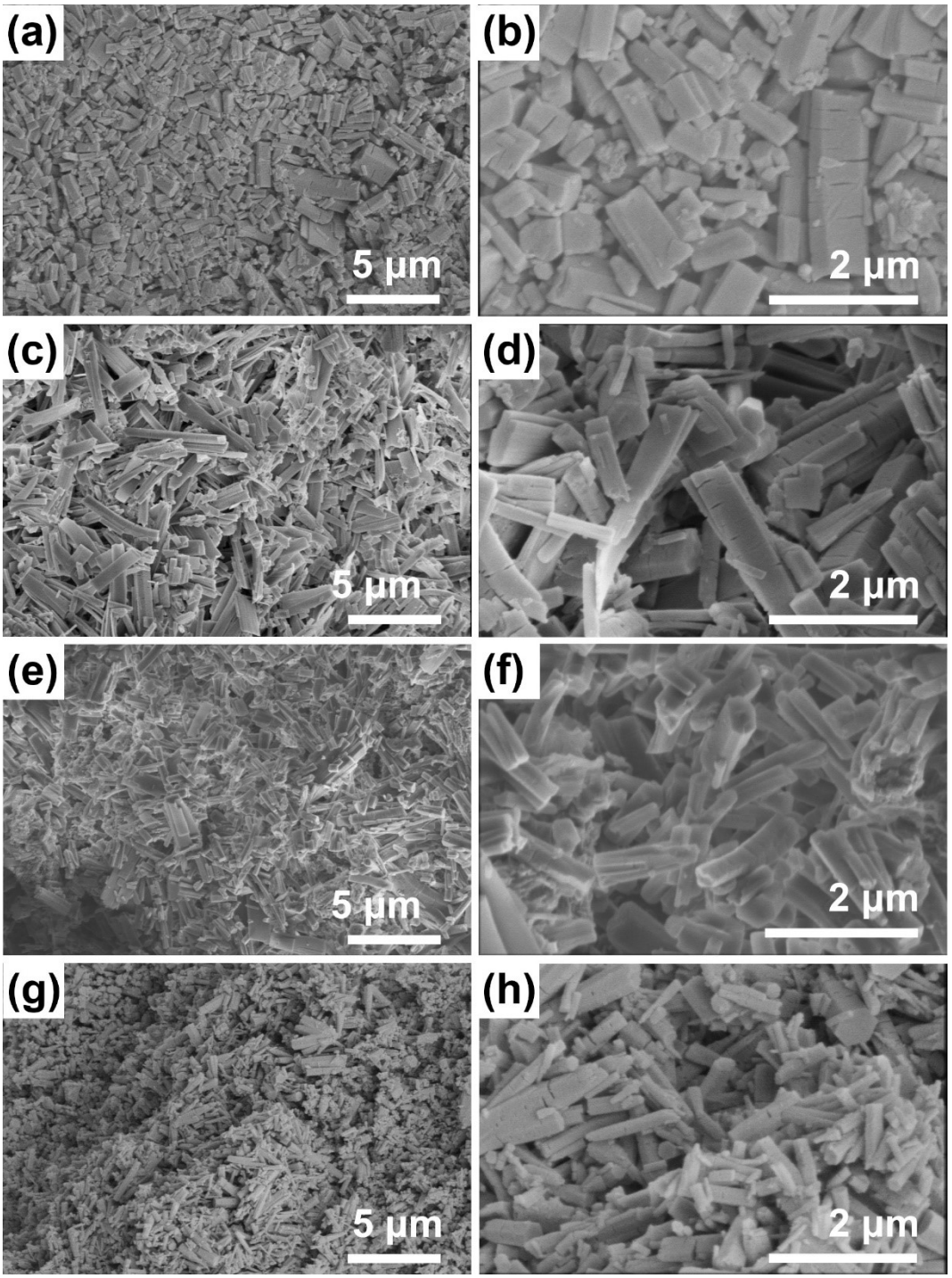

Fig. S2 SEM images of (a, b) $MeCl_{0.2}$, (c, d) $MeCl_{0.4}$, (e, f) $MeCl_{0.6}$, and (g, h) $MeCl_{0.8}$ at different magnifications.

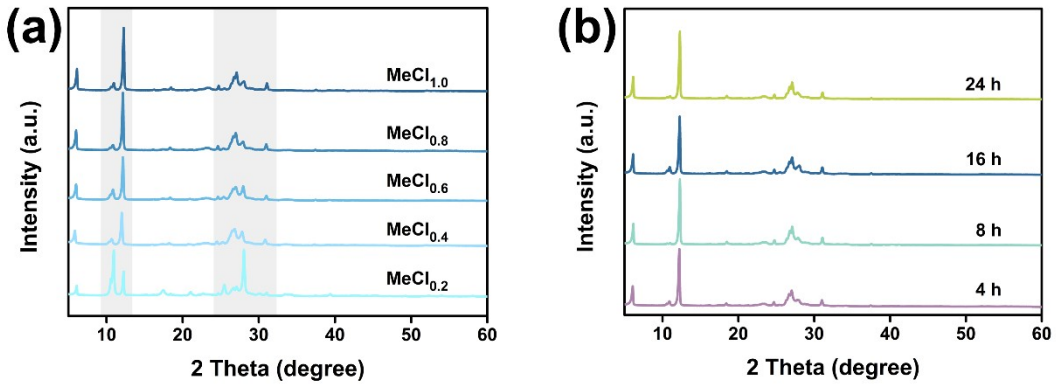

Fig. S3 (a) XRD patterns of $MeCl_x$ synthesized in aqueous solutions of different HCl concentrations; (b) XRD patterns of $MeCl_{1.0}$ synthesized with different shaking times.

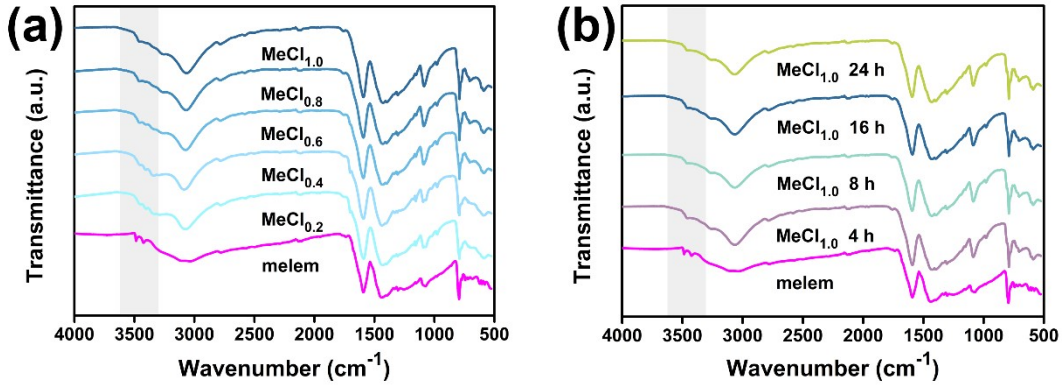

Fig. S4 (a) FTIR spectra of $MeCl_x$ synthesized in aqueous solutions of different HCl concentrations; (b) FTIR spectra of $MeCl_{1.0}$ synthesized with different shaking times. Untreated bulk melem for comparison (bottom, magenta spectra)

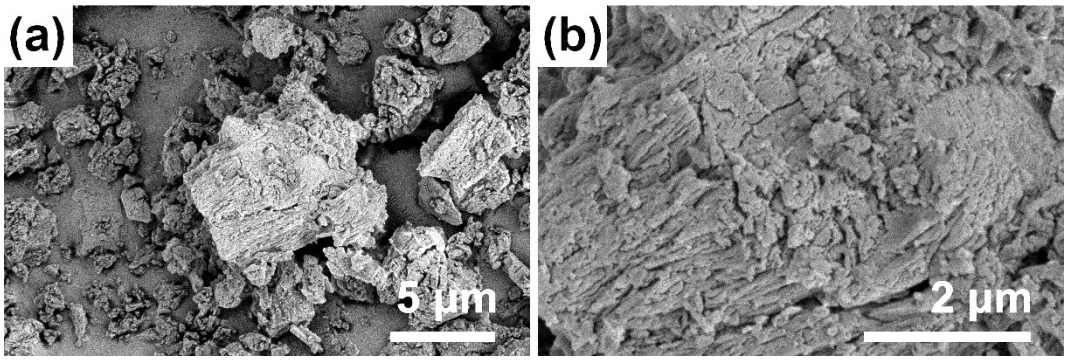

Fig. S5 SEM images of unwashed HCl-treated melem (melem+HCl) at different magnifications.

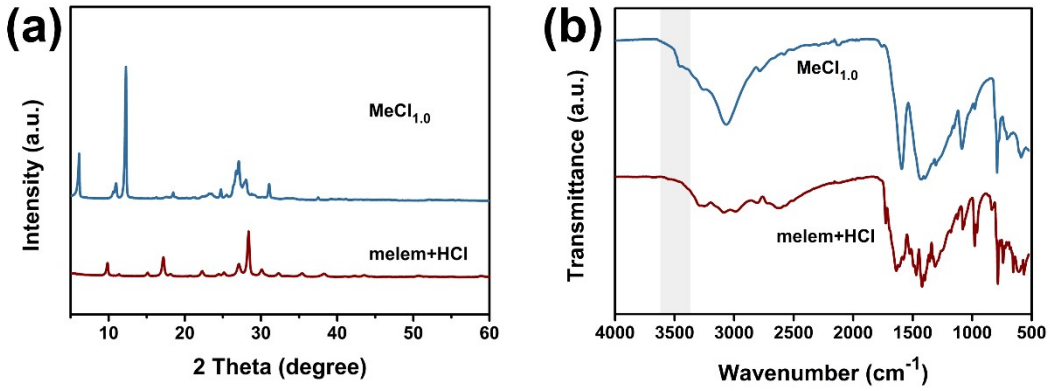

Fig. S6 (a) XRD patterns and (b) FTIR spectra of $MeCl_{1.0}$ and unwashed HCl-treated melem (melem+HCl).

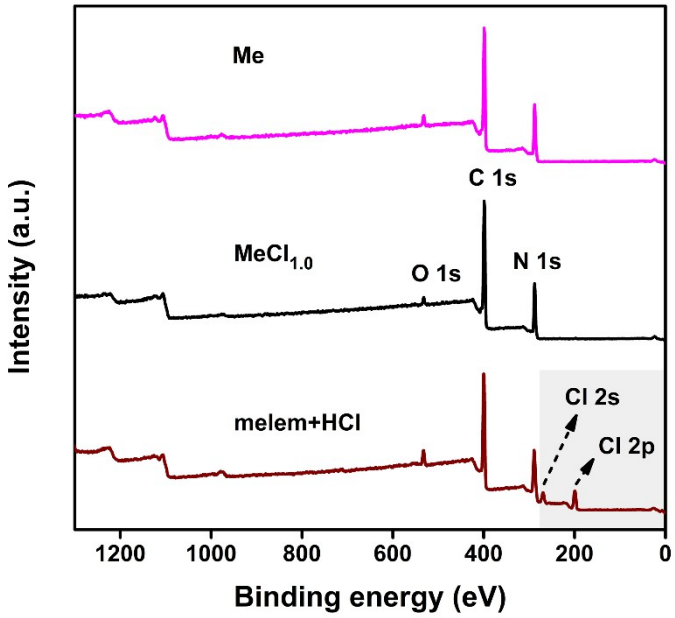

Fig. S7 Global XPS spectra of Me, $MeCl_{1.0}$, and melem+HCl.

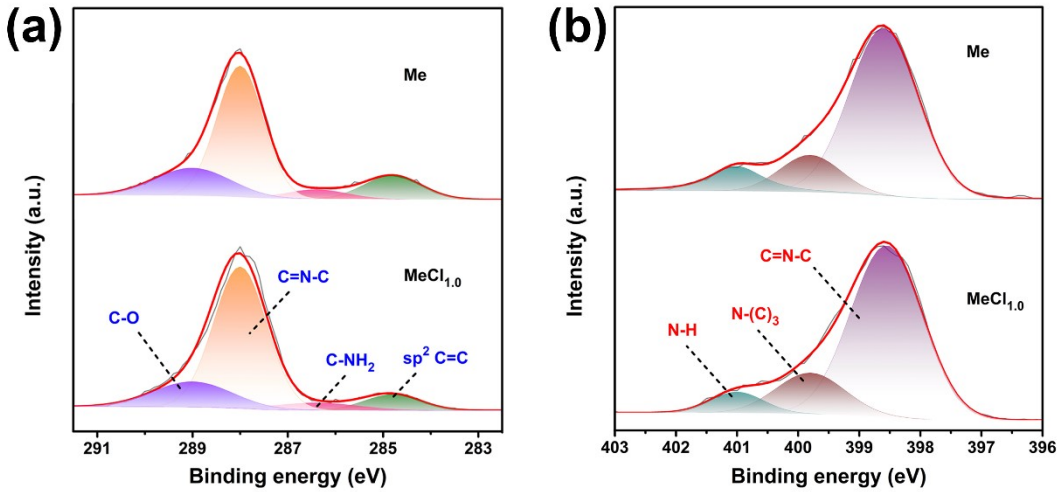

Fig. S8 (a) C 1s and (b) N 1s high-resolution XPS spectra of Me and $MeCl_{1.0}$.

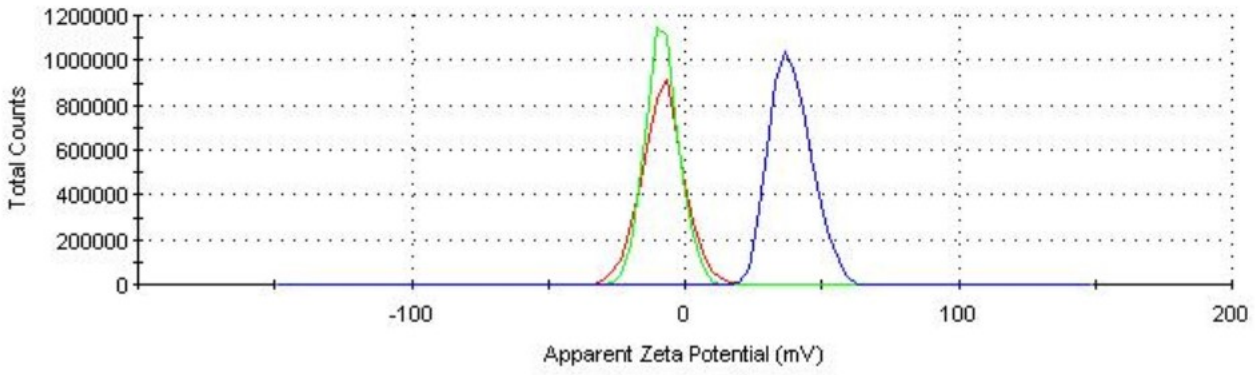

Fig. S9 Zeta-potential measurements of Me (green), $MeCl_{1.0}$ (red), and melem+HCl (blue) aqueous suspensions.

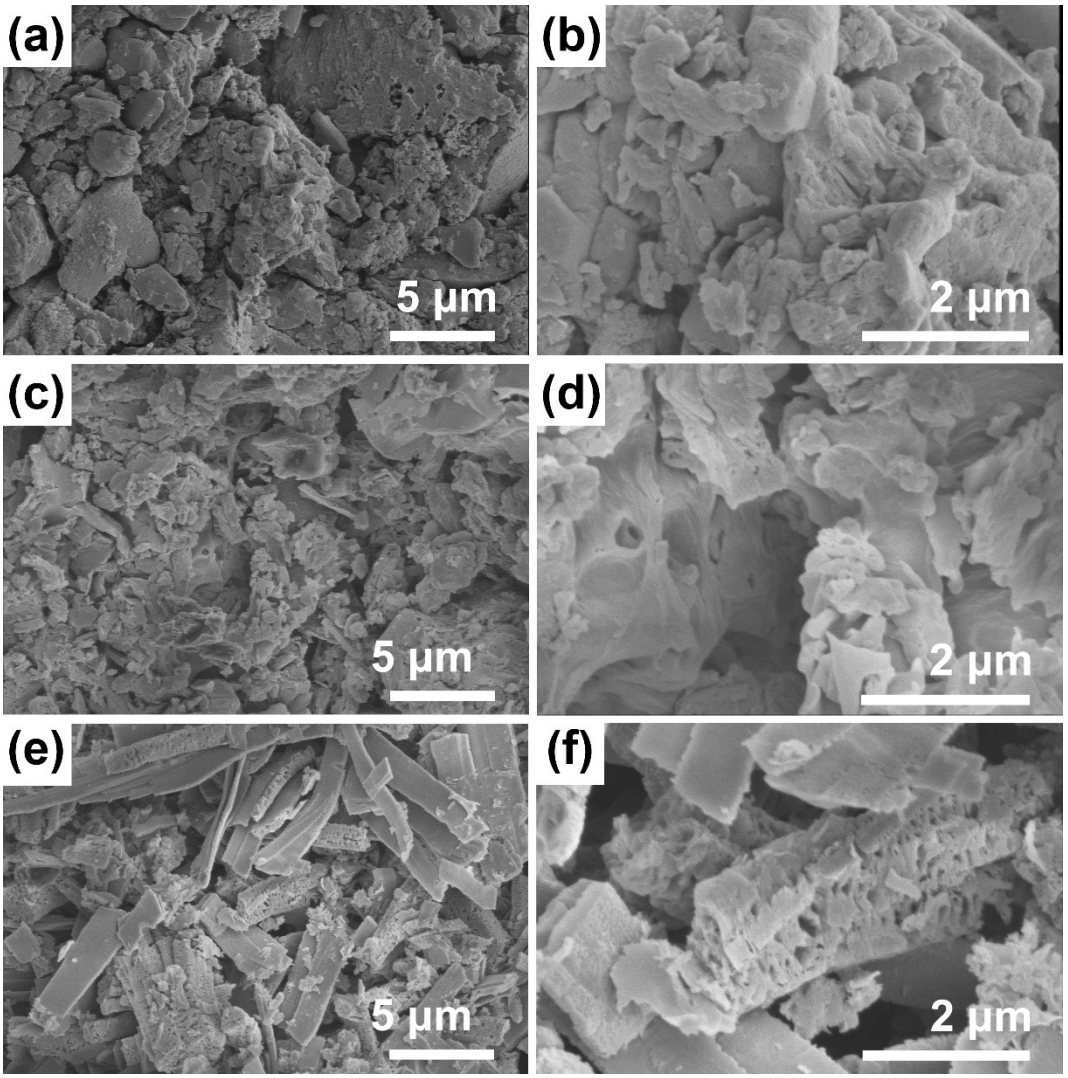

Fig. S10 SEM images of (a, b) CN-M, (c, d) CN-melem, and (e, f) CN-Me at different magnifications.

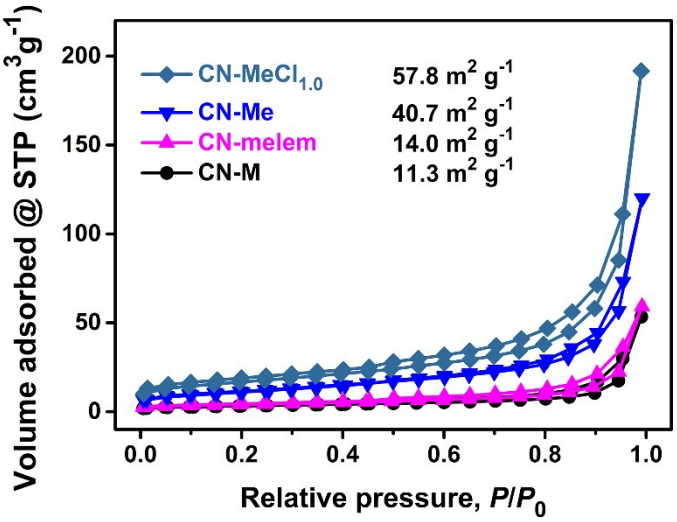

Fig. S11 Nitrogen adsorption-desorption isotherms (77 K) and specific surface area analysis according to the Brunauer-Emmett-Teller (BET) model.

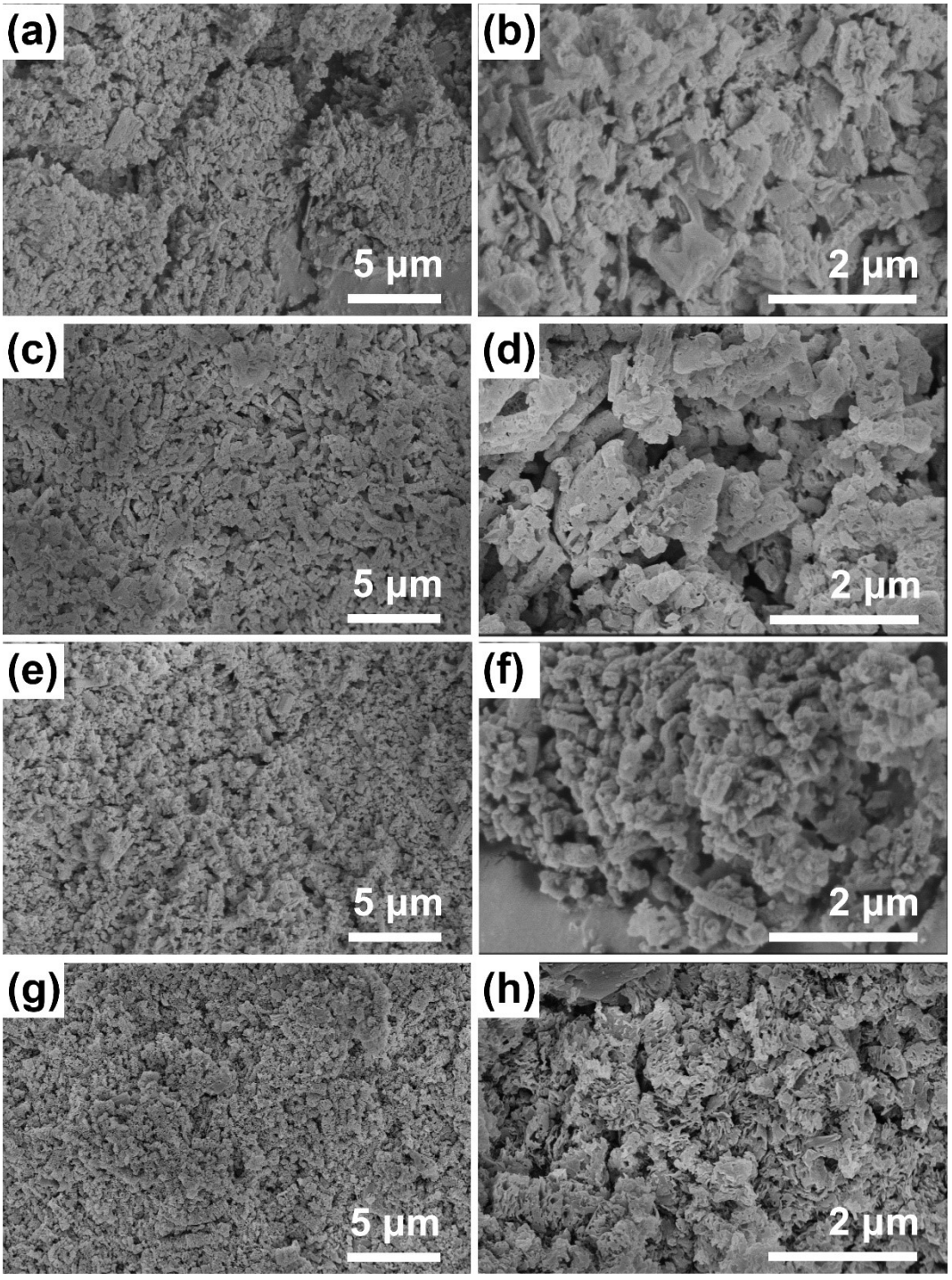

Fig. S12 SEM images of (a, b) CN-$MeCl_{0.2}$, (c, d) CN-$MeCl_{0.4}$, (e, f) CN-$MeCl_{0.6}$, and (g, h) CN-$MeCl_{0.8}$ at different magnifications.

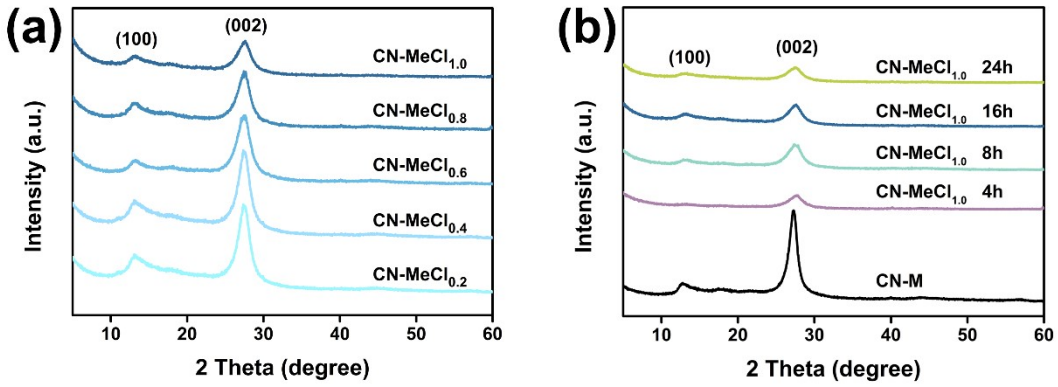

Fig. S13 (a) XRD patterns of CN materials from $MeCl_x$, synthesized in aqueous solutions of different HCl concentrations; (b) XRD patterns of CN-M compared with CN materials from $MeCl_{1.0}$ synthesized with different shaking times.

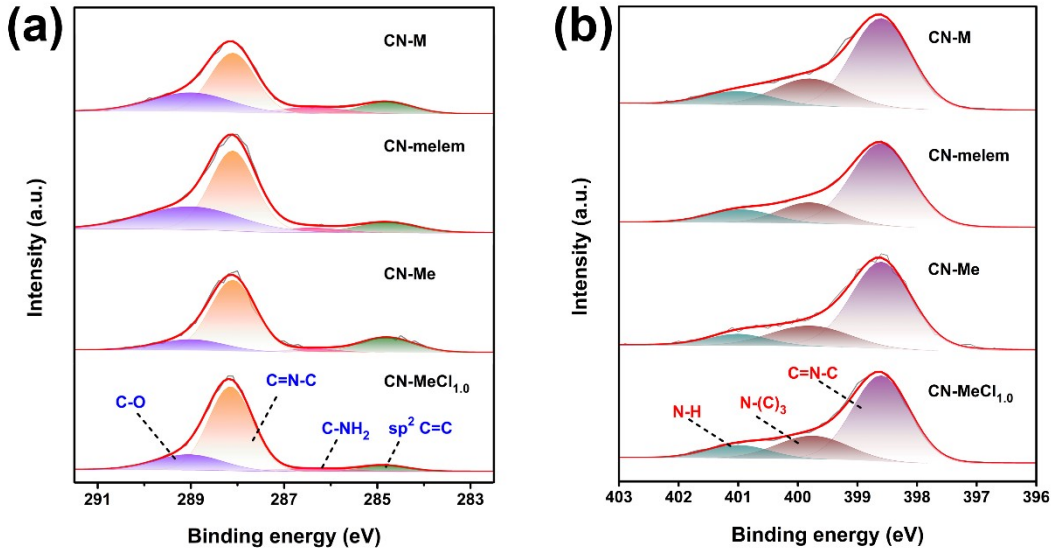

Fig. S14 (a) C 1s and (b) N 1s high-resolution XPS spectra of CN-M, CN-melem, CN-Me, and CN-$MeCl_{1.0}$.

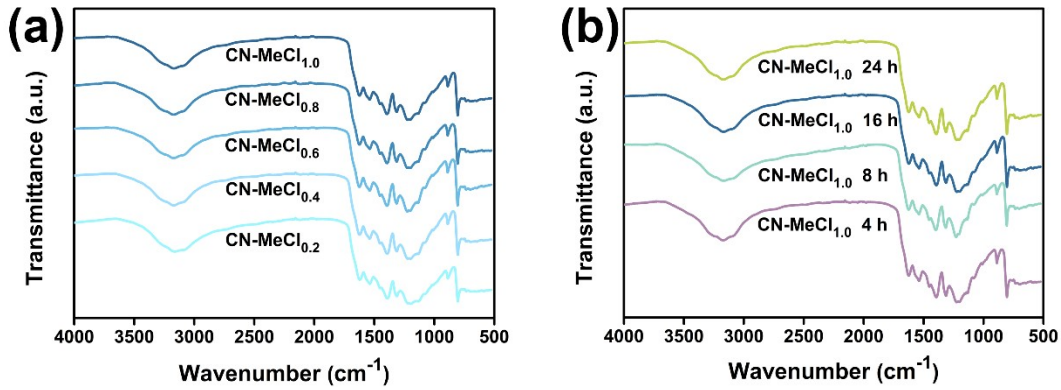

Fig. S15 (a) FTIR spectra of CN materials from $MeCl_x$, synthesized in aqueous solutions of different HCl concentrations; (b) FTIR spectra of CN materials from $MeCl_{1.0}$ synthesized with different shaking times.

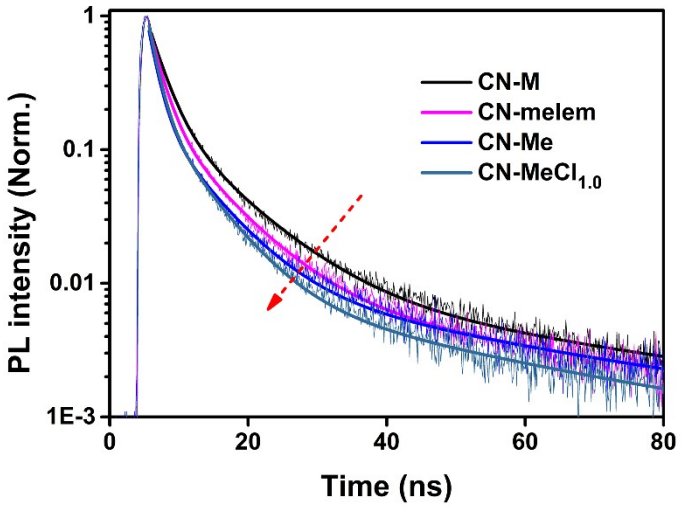

Fig. S16 Normalized time-resolved PL decay spectra of different CN materials (all samples were excited at λ_{ex} = 370 nm).

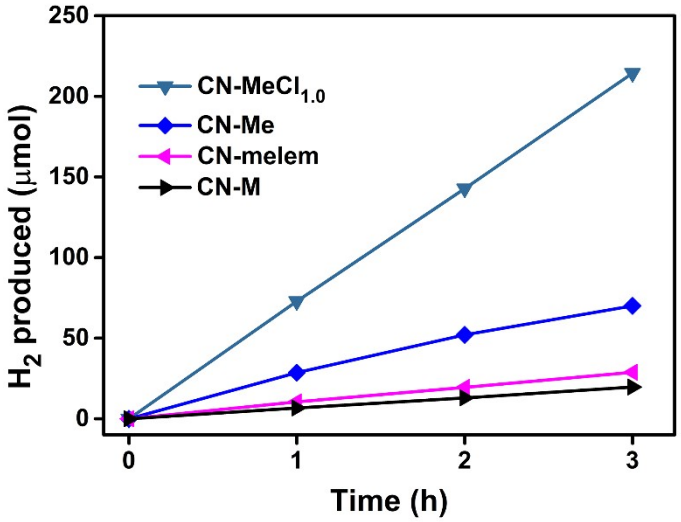

Fig. S17 Time course of H_2 evolution under white LED irradiation, catalyzed by different CN materials.

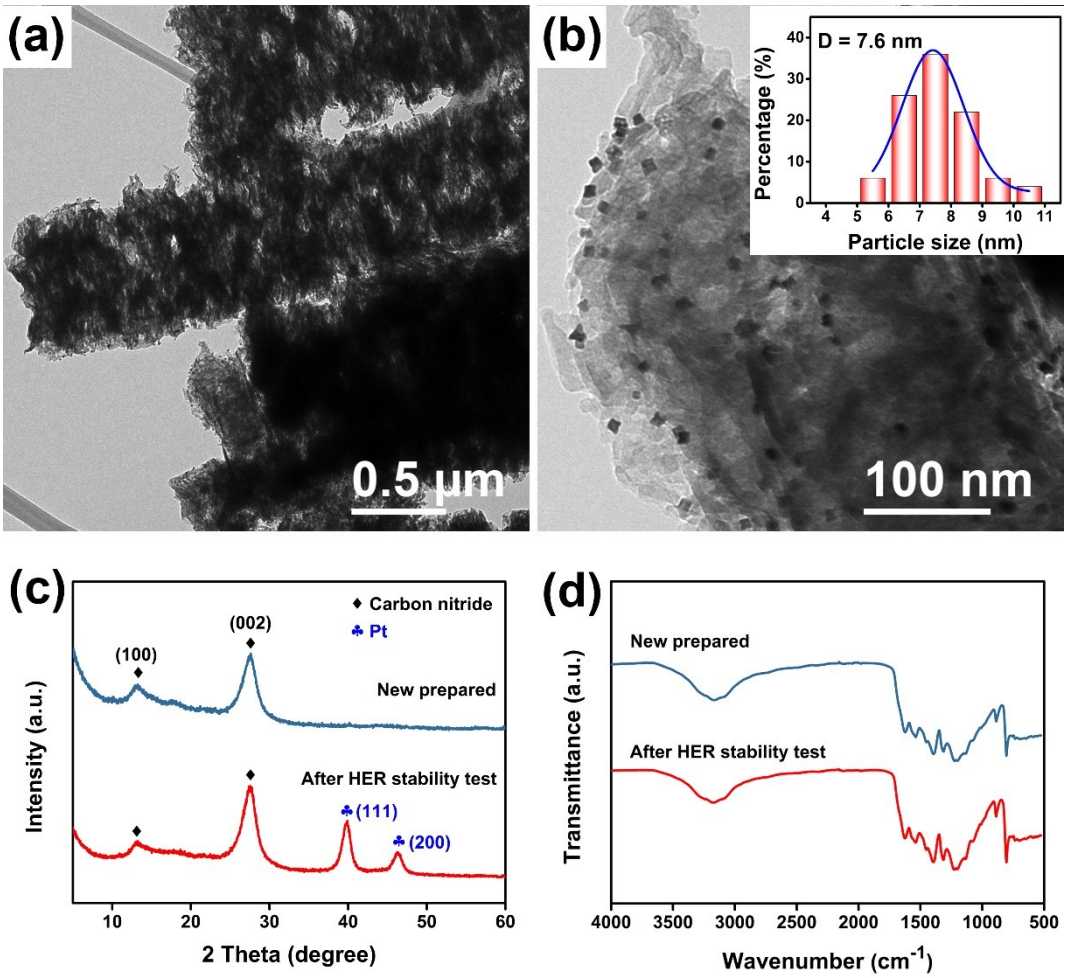

Fig. S18 (a,b) TEM images of CN-$MeCl_{1.0}$ at two different magnifications after an HER stability test. The inset in (b) presents a size distribution historgram of Pt nanoparticles; (c) XRD patterns and (d) FTIR spectra of CN-$MeCl_{1.0}$ before and after HER stability test.

The two diffraction peaks located at 2θ = 39.8° and 2θ = 46.2° are assigned to the (111) and (200) planes of face center cubic (fcc) Pt nanoparticles, which are photodeposited onto the surface of CN material. The XRD patterns and FTIR spectra of CN-$MeCl_{1.0}$ do not reveal noticeable change before and after HER stability test, indicating a good structural stability.

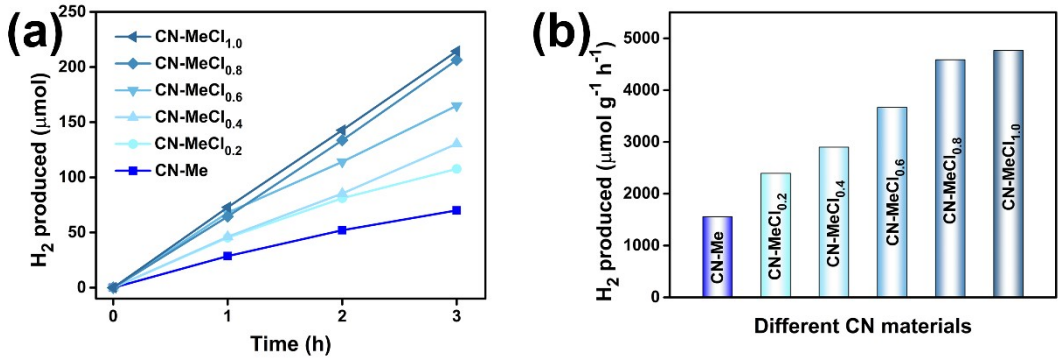

Fig. S19 (a) Time course of H_2 evolution under white LED irradiation, catalyzed by CN materials synthesized in aqueous solutions of different HCl concentrations; (b) The corresponding HER rate at the 3rd hour.

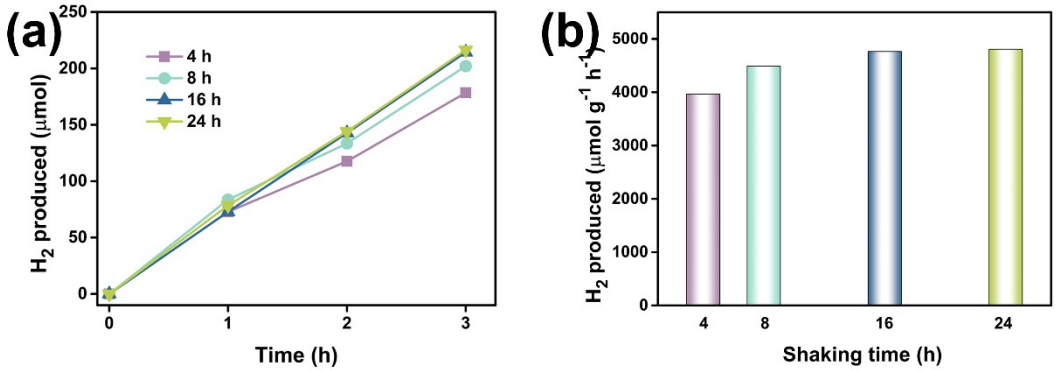

Fig. S20 (a) Time course of H_2 evolution under white LED irradiation, catalyzed by CN materials synthesized from $MeCl_{1.0}$ with different shaking times; (b) Corresponding HER rate at the 3rd hour.

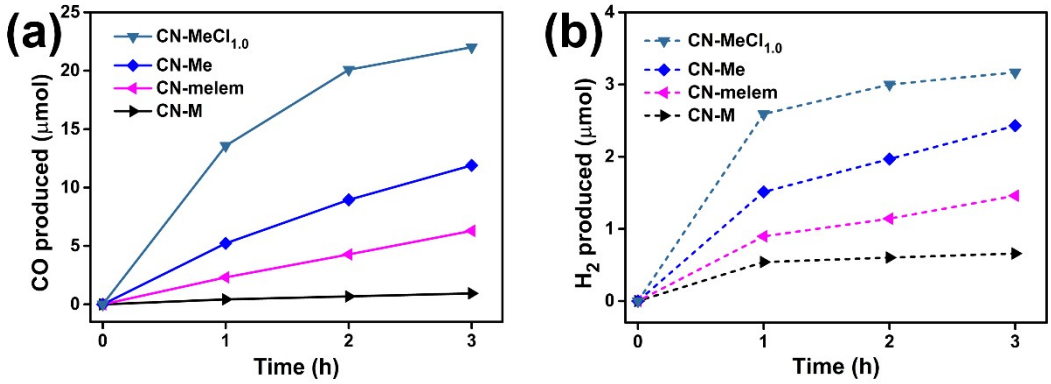

Fig. S21 Time course of generated (a) CO and (b) H_2 under white LED irradiation, catalyzed by different CN materials.

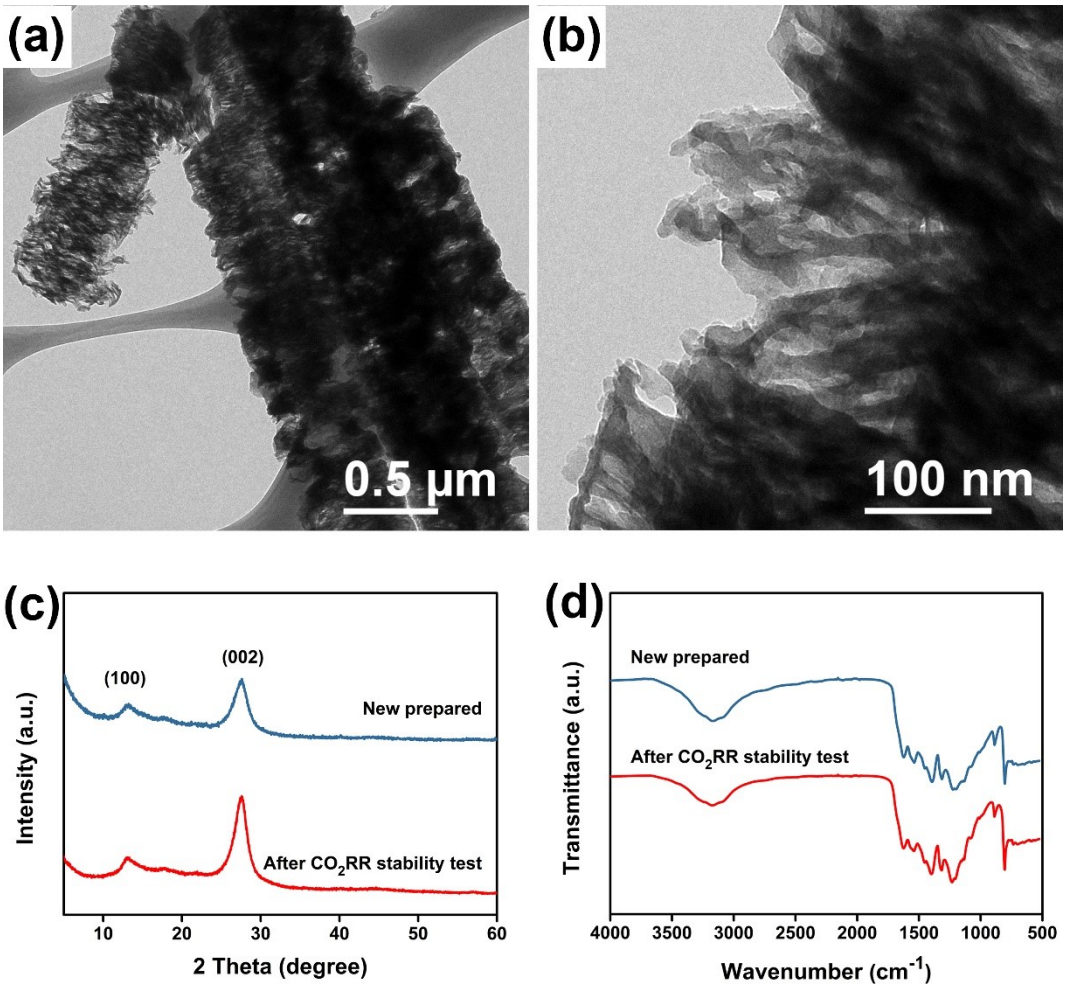

Fig. S22 (a, b) TEM images of CN-$MeCl_{1.0}$ after CO_2RR stability test at two different magnifications; (c) XRD patterns and (d) FTIR spectra of CN-$MeCl_{1.0}$ before and after CO_2RR stability test.

The XRD patterns and FTIR spectra of CN-$MeCl_{1.0}$ do not reveal a noticeable change before and after a HER stability test, indicating a good structural stability.

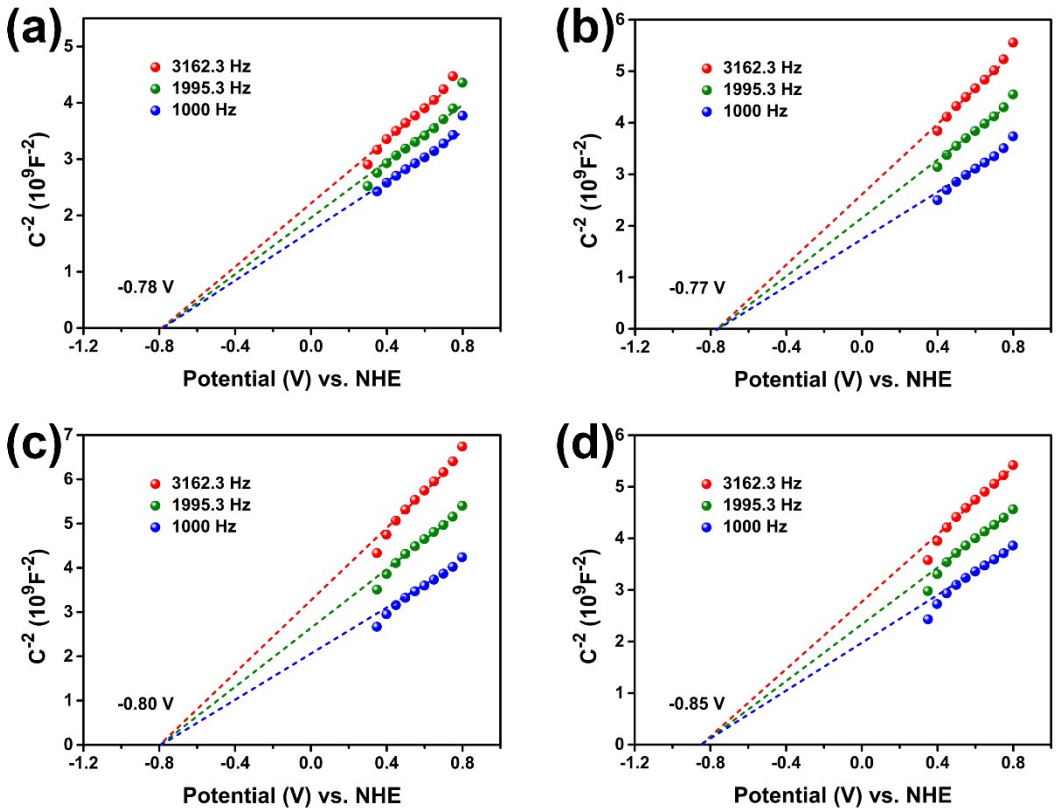

Fig. S23 Mott-Schottky plots of (a) CN-M, (b) CN-melem, (c) CN-Me, and (d) CN-$MeCl_{1.0}$, measured in 1.0 M Na_2SO_4 aqueous solution as the electrolyte.

Table S1. PL lifetimes estimated from time-resolved PL spectra decay curves according to a triple-exponential function fitting.

Catalyst	τ_1 (ns)	A_1 (%)	τ_2 (ns)	A_2 (%)	τ_3 (ns)	A_3 (%)	$\tau_{av.}$ (ns)
CN-M	8.24	45.91	49.53	16.33	2.16	37.76	34.17
CN-melem	1.75	35.87	7.11	47.19	45.64	16.95	32.26
CN-Me	1.32	24.24	6.17	46.86	39.03	18.91	28.58
CN-$MeCl_{1.0}$	5.68	47.33	34.98	14.91	1.32	37.76	23.61

The PL lifetimes ($\tau_{av.}$) were estimated from time-resolved PL spectra decay curves fitted to a triple-exponential function: $\tau = \sum_{i=1}^{i=n} A_i \tau_i^2 / \sum_{i=1}^{i=n} A_i \tau_i$, where τ_i is the lifetime and A_i is the amplitude of the i^{th} component.

Table S2. Comparison of the properties of CN materials used as HER photocatalysts

Catalyst	Method	Light source	Catalyst mass	Experimental conditions	Hydrogen evolution rate (μmol g^{-1} h^{-1})	AQE (%)	Ref.
CN from melem-based supramolecular hexagonal rods	Supramolecular assembly of melem exfoliated by HCl, followed by thermal condensation	100 W white LED (λ > 410 nm), water bath	15 mg	3 wt.% Pt, 10 vol.% TEOA	4764	6.8 (λ = 405 nm)	This work
Porous CN	Thermal condensation of melamine-halogen complex	50 W white LED (λ > 410 nm)	15 mg	3 wt.% Pt, 10% vol.% TEOA	1815	3.2 (λ = 405 nm)	[1]
Hierarchical rod-like graphitic CN	Ultrasound-assisted supramolecular assembly of melem, followed by thermal condensation	300 W Xe lamp (λ > 420 nm)	100 mg	3 wt.% Pt, 10% vol.% TEOA	2460	—	[2]
Graphene-like CN rich in N vacancies	Thermal polymerization of melamine using graphene oxide as a sacrificial template	300 W Xe lamp (λ > 420 nm)	100 mg	3 wt.% Pt, 25% vol.% methanol	3171	~6 (λ = 421 nm)	[3]
High crystalline CN	Rapid polymerization of melamine powder	300 W Xe lamp (λ > 420 nm)	50 mg	3 wt.% Pt, 10 vol.% TEOA	339.4	3.8 (λ = 420 nm)	[4]
Macroscopic foam-like holey ultrathin CN nanosheets	Self-modification of polymeric melon units through long-time thermally treating bulk g-C_3N_4 under an air atmosphere	300 W Xe lamp (λ > 400 nm)	20 mg	3 wt.% Pt, 10 vol.% TEOA	1144	4.03 (λ = 420±15 nm)	[5]
Crystalline CN	Condensation of melamine powder, followed by a sequential heating in KCl-LiCl mixed sault	300 W Xe lamp	50 mg	3 wt.% Pt, 10 vol.% TEOA	1280	~6.0 (λ = 405 nm)	[6]
Holey CN nanosheets	Condensation of melamine powder in a big crucible with empty space covered with two Z204 catalysts	300 W Xe lamp (λ > 400 nm)	50 mg	3 wt.% Pt, 10 vol.% TEOA	2320	—	[7]
Defect engineering-modified atomic layered CN	High-temperature treatment and the two-step thermal exfoliation process	Xe lamp (λ > 420 nm)	50 mg	3 wt.% Pt, 10 vol.% TEOA	3700	14.98 (λ > 420 nm)	[8]
Polymeric CN nanotubbes	Condensation of trithiocyanuric acid-melamine supramolecular assembly, followed by further heating treatment in NaCl salt	300 W Xe lamp (λ > 420 nm)	50 mg	1 wt.% Pt, 10 vol.% TEOA	4350	3.34 (λ = 420 nm)	[9]
Phenyl-bridged porous and hollow CN sphere	Condensation of trimesic acid-doped cyanuric acid-melamine supramolecular assembly	300 W Xe lamp (λ > 400 nm)	20 mg	3 wt.% Pt, 10 vol.% TEOA	4455	—	[10]

Electronic Supplementary Information References

[1] J. Barrio, A. Grafmüller, J. Tzadikov, M. Shalom, *Appl. Catal. B*, 2018, **237**, 681.

[2] Z. Huang, F. -W. Yan, G. -q. Yuan, *ACS Sustainable Chem. Eng.*, 2018, **6**, 3187.

[3] R. Wang, X. Wang, X. Li, L. Pei, X. Gu, Z. Zheng, *Int. J. Hydrogen Energy*, 2021, **46**, 197.

[4] L. Wang, Y. Hong, E. Liu, Z. Wang, J. Chen, S. Yang, J. Wang, X. Lin, J. Shi, *Int. J. Hydrogen*

Energy, 2020, **45**, 6425.

[5] Y. Li, R. Jin, Y. Xing, J. Li, S. Song, X. Liu, M. Li, R. Jin, *Adv. Energy Mater.*, 2016, **6**, 1601273.

[6] W. Ren, J. Cheng, H. Ou, C. Huang, M.M. Titirici, X. Wang, *ChemSusChem*, 2019, **12**, 3257.

[7] G. Li, Z. Xie, S. Chai, X. Chen, X. Wang, *Appl. Catal. B*, 2021, **283**, 119637.

[8] J. Zhang, J. Chen, Y. Wan, H. Liu, W. Chen, G. Wang, R. Wang, *ACS Appl. Mater. Interfaces*, 2020, **12**, 13805.

[9] Y. Wan, J. Zhang, J. Chen, Z. Liu, J. Fan, J. Zhang, G. Wang, R. Wang, *Chem. Eng. J.*, 2021, **417**, 127956.

[10] Y. Chen, Y. Qu, X. Zhou, D. Li, P. Xu, J. Sun, *ACS Appl. Mater. Interfaces*, 2020, **12**, 41527.